1-1-1998

Removal of laser-melted material with an assist gas

K. Farooq
University of Central Florida

A. Kar
University of Central Florida

Removal of laser-melted material with an assist gas

Cite as: Journal of Applied Physics **83**, 7467 (1998); https://doi.org/10.1063/1.367509
Submitted: 18 December 1997 . Accepted: 11 March 1998 . Published Online: 28 May 1998

K. Farooq, and A. Kar

Removal of laser-melted material with an assist gas

K. Farooq and A. Kar[a)]
Center for Research & Education in Optics and Lasers (CREOL), Mechanical, Materials and Aerospace Engineering Department, University of Central Florida, 4000 Central Florida Boulevard, Orlando, Florida 32816-2700

(Received 18 December 1997; accepted for publication 11 March 1998)

Molten material is removed in many laser applications such as laser grooving and laser cutting. An assist gas is usually used to remove the molten material from the laser material interaction zone. The effect of assist gas pressure on the material removal rate is investigated in this article for laser cutting and grooving applications. The model for melt depth is based on the overall energy balance, and the cut depth is obtained by considering the effect of the assist gas. The model for kerf width is based on the modified Rosenthal solution taking into account the melting effect. The cut depths reach a constant value beyond a critical pressure if the kerf width is of the order of nozzle width and through cuts are assumed. Most of the molten material is removed by the assist gas at pressures below this critical pressure. The model predicts on the basis of the Prandtl or Meyer relation that the cutting speed decreases when the assist gas pressure exceeds a critical value if the kerf dimensions are smaller than the nozzle dimensions.
[S0021-8979(98)00912-8]

I. INTRODUCTION

Melt removal during laser materials processing is modeled in this study, and the model results are compared to experimental data for a chemical oxygen–iodine laser (COIL) of wavelength 1.315 μm. The basic principle of COIL has been discussed briefly by Kar *et al.*[1] Two important applications of melt removal are laser cutting and laser grooving. The effects of assist gas pressure on laser cutting have been studied by Chryssolouris and Choi,[2] Biermann *et al.*,[3] and Molian and Baldwin.[4] Schuocker and Abel[5] presented a mathematical model for the material removal process during laser cutting. The physical mechanism of the process has been discussed by Schuocker.[6] Mathematical models for the evaporative cutting have been developed by Modest and Abakian,[7] Bang and Modest,[8] and Roy and Modest.[9] Belic and Stanic,[10] and Belic[11] analyzed the laser cutting process with a simple model involving empirical parameters. The purpose of this article is to model the effects of assist gas pressure on the cut depth and kerf width. This work is based on the model in Ref. 12 where several physical effects such as the convection and shock wave phenomena have been neglected. These effects are analyzed in this study to show that the cutting speed decreases when the assist gas pressure is increased above a critical value leading to the shock formation above the substrate surface.

II. MATHEMATICAL MODEL FOR MELT AND CUT DEPTHS

A. Energy and mass balance equations

The proposed model is based on the lumped parameter technique[12] in which the overall energy and mass balances are considered instead of the pointwise distribution. The overall energy and mass balance equations are, respectively, written as

$$\begin{aligned} AP\tau = {} & \rho w_k(d_m-d_c)(v+V_m)\tau[c_p(T_m-T_0)+L_m \\ & +c_p(T_a-T_m)]+\rho w_k d_m v\tau\beta L_b \\ & +f_d\rho v w_k d_m\tau[c_p(T_m-T_0)+L_m+c_p(T_a-T_m)] \\ & +E_{\mathrm{cond}}+E_{\mathrm{conv}}, \end{aligned} \tag{1}$$

$$\rho w_k v d_m\tau=\rho w_k(v+V_m)(d_m-d_c)\tau+f_d\rho w_k v d_m\tau. \tag{2}$$

The mass of the metal vapor is not included in the mass balance Eq. (2) because it is very small as compared to the mass of the melt. The first, second, and third terms on the right side of Eq. (1) represent the total amount of material processed (melted and boiled). The first term accounts for the energy associated with the material that leaves the depressed region at the base of the kerf as shown in the Fig. 1, as a result of the impinging jet; whereas the second term accounts for the energy required to boil a fraction of the molten material. The third term accounts for the energy loss as a result of the splashing or entrainment of molten droplets by the assist gas, and the sticking of molten layers to the side walls of the kerf. f_d denotes a fraction of the total amount of material melted by the laser beam. E_{cond} is the energy loss from the melt to the surrounding solid region in the workpiece due to heat conduction. E_{conv} is the convective heat loss from the melt to the assist gas at the free surface of the liquid metal. P is the power of incident laser beam and A is the absorptivity of the substrate. T_m, T_a, and T_0 are, respectively, the melting temperature, characteristic temperature of the melt pool, and ambient temperature. d_m and d_c represent the melt and cut depths respectively. L_m, L_b, c_p, and V_m are, respectively, the latent heat of melting, latent heat of boiling, specific heat capacity of the substrate at constant

[a)]Electronic mail: aravinda@lorien.creol.ucf.edu

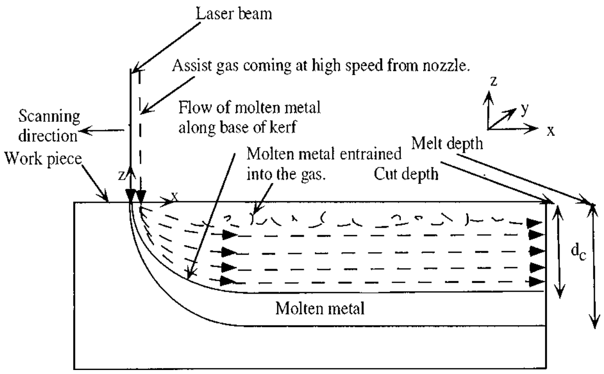

FIG. 1. High speed assist gas is carving out a kerf in molten metal.

pressure, and the average velocity of liquid metal in the kerf. The laser-substrate interaction time is defined as $\tau = l/v$ where l is the length of the rectangular laser spot and v is the scanning velocity. l is measured in the scanning direction.

The energy loss due to the heat conduction is determined by using the Fourier law of heat conduction and is given by the following expression:[1]

$$E_{\mathrm{cond}} = d_m \left[\frac{w_k k + 2lk}{2(\alpha\tau)^{1/2}} \right] (T_m - T_0)\tau, \tag{3}$$

where k is the thermal conductivity and α is the thermal diffusivity of the workpiece.

Heat loss due to convection as a result of the assist gas flowing over the melt surface is given by

$$E_{\mathrm{conv}} = \bar{h} w_k d_m (T_s - T_u)\tau, \tag{4}$$

where T_s is the surface temperature of the melt and T_u is the temperature of the assist gas at the nozzle exit, which will be determined later. T_s is an unknown, however, it is taken to be the characteristic temperature of the melt, T_a, in the subsequent calculations. This overestimates the heat loss due to convection but the convection heat loss is still found to be insignificant as shown later. The average heat transfer coefficient, $\bar{h}$ is estimated by using the following expression that is applicable to a single slot nozzle[13]

$$\bar{h} = \frac{3.06 Pr^{0.42} Re^m k_g}{D_h \left[\dfrac{y}{W} + \dfrac{H}{W} + 2.78 \right]} \quad \text{for} \quad \left[\begin{array}{c} 3000 \leqslant Re \leqslant 90\,000 \\ 2 \leqslant H/W \leqslant 10 \\ 4 \leqslant y/W \leqslant 20 \end{array} \right], \tag{5a}$$

where

$$m = 0.695 - \left[\left(\frac{y}{2W} \right) + \left(\frac{H}{2W} \right)^{1.33} + 3.06 \right]^{-1}. \tag{5b}$$

Pr and k_g are, respectively, the Prandtl number and thermal conductivity of the gas. y is the perpendicular distance from the line running lengthwise through the center of the nozzle. W is the width of the nozzle and H is the height of the nozzle from the workpiece. The Reynolds number, Re is given by $Re = V_g' D_h / v_g$, where V_g' and v_g are, respectively, the velocity and kinematic viscosity of the gas at the nozzle exit. The hydraulic diameter, D_h is given by $D_h = 4A_c/P_c$, where A_c and P_c are the cross-sectional area and perimeter of the nozzle, respectively. k_g, v_g, and Pr are evaluated at one atmospheric pressure and temperature T_u.

B. Gas dynamic analysis for the assist gas

The assist gas expands after leaving the nozzle depending on the ambient pressure, and its velocity, V_g' is given by[14,15]

$$V_g' = M_j^* \sqrt{\frac{2\gamma}{\gamma+1} R T_0} \quad \text{for } j = u \text{ or } d \text{ as discussed below,} \tag{6}$$

where γ is the specific heat ratio which is also known as the isentropic index. It is given by $\gamma = c_p'/c_v'$ where c_p' and c_v' are the specific heat capacities of the assist gas at constant pressure and volume, respectively. For diatomic gases such as nitrogen, $\gamma = 1.4$. R is the universal gas constant and T_0 is the room temperature which is taken as 300 K in this study. M_j^* is a dimensionless velocity of the assist gas depending on its flow conditions. The critical pressure, P^*, is defined as

$$P^* = P_0 \left[\frac{\gamma+1}{2} \right]^{\frac{\gamma}{\gamma-1}}$$

where P_0 is the ambient pressure. Depending on the assist gas pressure at the nozzle mouth, P_n, three kinds of flow situations of interest are listed below.

(i) Supersonic flow ($P_n > P^*$) in which the shock wave is formed between the nozzle and substrate surface: This may occur in grooving, or through cuts of small kerf width relative to the nozzle dimensions. The dimensionless velocity at the upstream of the shock wave is given by[14]

$$M_u^{*2} = \frac{(\gamma+1)}{(\gamma-1)} \left[1 - \left(\frac{P_0}{P_n} \right)^{\frac{\gamma-1}{\gamma}} \right]. \tag{7}$$

The dimensionless velocity at the downstream of the shock wave, M_d^* is given by the Prandtl or Meyer relation,[16] $M_d^* = 1/M_u^*$. It should be noted that the dimensionless velocity at the upstream of the shock front is taken equal to the dimensionless velocity at the nozzle exit. The velocity with which the assist gas enters the kerf is obtained from Eq. (6) by setting $M_j^* = M_d^*$. The dimensionless velocity M_j^* is related to the Mach number M_j through the following relation:[15]

$$M_j^2 = \frac{\dfrac{2}{\gamma+1} M_j^{*2}}{1 - \dfrac{\gamma-1}{\gamma+1} M_j^{*2}}, \tag{8}$$

where $j = u$ or d signifies the upstream and downstream conditions, respectively. The temperatures T_u and T_d of the assist gas at the upstream and downstream of shockfront, respectively, are given by the following expressions:[15]

$$\frac{T_0}{T_j} = 1 + \frac{\gamma-1}{2} M_j^2, \quad j = u \text{ or } d \tag{9}$$

(ii) Supersonic flow ($P_n > P^*$) in which the shock wave is formed at the kerf inlet: The velocity V_g' at the nozzle exit is obtained from Eq. (6) by setting $M_j^* = M_u^*$. The flow will be sonic inside the kerf even though the flow is supersonic outside the kerf. This situation is encountered for through cuts of uniform width comparable to the nozzle width. This is the maximum gas velocity that can be attained in the kerf for material removal to achieve the highest cutting rate.

(iii) Subsonic flow ($P_n < P^*$): The velocity V_g' at the nozzle exit is obtained from Eq. (6) by setting $M_j^* = M_u^*$. In through cuts, the velocity of the gas inside the kerf can be calculated by treating the kerf as a convergent or divergent nozzle if the kerf tapers in or out, respectively.

C. Melt flow

The assist gas removes the energy from the laser-material interaction zone through two mechanisms: (i) Surface effect which involves the convective cooling at the free surface of the melt, and (ii) bulk effect which refers to the removal of energy contained in the melt that is flushed away by the assist gas. The average velocity of the molten metal is calculated by considering the Poiseuille flow of the melt.[17]

$$V_m = -\frac{1}{12\mu}\left(\frac{dp}{dx}\right) w_k^2 . \tag{10}$$

The viscosity of the molten metal, μ depends on temperature as $\mu = \mu_0 \exp[E/(RT_a)]$ where μ_0 and E are constants and their values can be found in Ref. 18. The pressure gradient dp/dx in the metal is estimated by taking it to be the pressure gradient of the assist gas as it flows over the melt surface. Corner flow theory is used to analyze the assist gas velocity. A stagnation point exists below the gas jet, and the gas accelerates as it moves away from this point. The velocity of an ideal fluid flowing along a 90° corner of stationary solid surface is given by[17,19] $V_c = V_g' l/H$ at a distance l from the stagnation point. In the present case of melt removal, the assist gas transfers momentum to the liquid metal to induce flow in the melt giving rise to a moving boundary for the gas flow instead of the stationary surface used in the corner flow theory. This will significantly reduce the assist gas velocity compared to the value of V_c given by the above expression. To account for this effect, V_c is taken to be $V_c = F V_g' l/H$ where F is a fraction $(0 < F \leqslant 1)$. The pressure gradient is approximated as follows by using the Bernoulli equation,

$$\frac{dp}{dx} \approx \frac{\Delta p}{l} = \frac{\rho_0 V_c^2}{2l} = \frac{\rho_0 l}{2}\left(\frac{F V_g'}{H}\right)^2, \tag{11}$$

where ρ_0 is taken as the density of the assist gas at one atmospheric pressure and temperature 300 K.

The characteristic temperature of the melt, T_a in Eqs. (1) and (4) is obtained by considering the Stefan condition at the solid–liquid interface which yields[1]

$$T_a - T_m = \epsilon \frac{\rho L_m}{2kl} v w_k + \epsilon \frac{T_m - T_0}{2(\alpha l w_k)^{1/2}} (v w_k)^{1/2}. \tag{12}$$

ϵ is the average thickness of the recast layer in the kerf and is taken to be 0.1 mm in this study. Combining Eqs. (1) and (2) and utilizing Eqs. (3), (4), and (12), the melt depth is found to be

$$\frac{d_m}{p} = \frac{A_0}{v w_k + A_1 (v w_k)^2 + A_2 (v w_k)^{3/2} + A_3 (v w_k)^{1/2} + A_4 (h v w_k^2) + A_5 (h v^{1/2} w_k^{3/2}) + A_6 h w_k}, \tag{13}$$

where the coefficients are defined as

$$A_0 = \frac{A}{a_0}, \tag{14a}$$

$$A_1 = \frac{\rho^2 c_p L_m \epsilon}{2 a_0 k l}, \tag{14b}$$

$$A_2 = \frac{\rho \epsilon c_p (T_m - T_0)}{2 a_0 (\alpha l w_k)^{1/2}}, \tag{14c}$$

$$A_3 = \left[\frac{w_k k + 2kl}{2 a_0 (\alpha l w_k)^{1/2}}\right](T_m - T_0), \tag{14d}$$

$$A_4 = \frac{\rho L_m \epsilon}{2 a_0 k l}, \tag{14e}$$

$$A_5 = \frac{\epsilon (T_m - T_0)}{2 a_0 (\alpha l w_k)^{1/2}}, \tag{14f}$$

$$A_6 = \frac{(T_m - T_u)}{a_0}, \tag{14g}$$

and

$$a_0 = \rho [c_p (T_m - T_0) + L_m + \beta L_b]. \tag{14h}$$

For a rectangular laser spot of length $l = 1.7$ mm and width $w = 1.2$ mm, the thermophysical data listed in Tables I and II and the assumptions that $T_0 = 300$ K, $\epsilon = 0.1$ mm, $\beta = 0.1$, and $w_k = w$, the coefficients in expressions Eqs. (14b)–(14h) are found to be $a_0 = 1.24 \times 10^{10}$ [J/m^3], $A_1 = 233.35$ [s/m^2], $A_2 = 3.29$ [s$^{1/2}$/m], $A_3 = 0.0033$ [m/s$^{1/2}$], $A_4 = 6.50 \times 10^{-5}$ [m s K/J], $A_5 = 9.18 \times 10^{-7}$ [m^2 K s$^{1/2}$/J], and $A_6 = 1.26 \times 10^{-7}$ [m^3 K/J]. To carry out the order of magnitude analysis, these coefficients are multiplied by the respective terms to obtain $A_1 (v w_k)^2 = 1.34 \times 10^{-7}$ [m^2/s], $A_2 (v w_k)^{3/2} = 3.87 \times 10^{-7}$ [m^2/s], $A_3 (v w_k)^{1/2} = 1.62 \times 10^{-5}$ [m^2/s], $A_4 h v w_k = 2.07 \times 10^{-9}$ [m^2/s], $A_5 h v^{1/2} w^{3/2} = 1.46 \times 10^{-9}$ [m^2/s], and $A_6 h w_k = 1.67 \times 10^{-7}$ [m^2/s] where $v = 1.2$ m/s. The value of h is calculated for the largest nozzle of length 22 mm and

TABLE I. Typical values of thermophysical properties of iron. Due to the lack of availability of high temperature data, these values were used in this study to obtain various results for 400 series stainless steel workpiece.[a]

Thermophysical properties	Values of thermophysical properties
Density, ρ	7870 kg m^{-3}
Melting point, T_m	1809 K
Boiling point, T_b	3133 K
Specific heat, c_p	456 J Kg^{-1} K
Thermal conductivity, k	78.2 W m^{-1} K^{-1}
Thermal diffusivity, $\alpha=k/(\rho c_p)$	2.18×10^{-5} m^2 s^{-1}
Latent heat of melting, L_m	2.72×10^{5} J Kg^{-1}
Latent heat of boiling, L_b	6.10×10^{6} J Kg^{-1}
Dynamic viscosity, μ_0	0.3699 m N s m^{-2}
Activation Energy, E	41.4 kJ mol^{-1}

[a]See Ref. 18.

width $W=1$ mm for the conditions at which the assist gas attains sonic velocity at the kerf inlet. For this situation the temperature of the gas is found to be $T_u=250$ K by taking the Mach number $M_u=1$ in Eq. (9). The distance between the nozzle and workpiece (H) and the parameter y are taken as 6 and 20 mm, respectively, in Eq. (5a). The average value of the heat transfer coefficient is $h=1708$ [W/m^2 K] under these conditions. These magnitudes indicate that the terms involving A_3 is dominant in affecting the melt depth compared to the rest of the terms. Therefore, Eq. (13) can be simplified as

$$\frac{d_m}{P}=\frac{A_0}{v w_k+A_3(v w_k)^{1/2}}. \tag{15}$$

The assist gas removes the melt to produce a slot of depth d_c in the case of laser grooving. d_c is equal to the thickness of the workpiece for laser cutting applications. The mass balance Eq. (2) relates d_c to d_m as given below.

$$d_c=\left(\frac{V_m+f_d v}{V_m+v}\right)d_m. \tag{16}$$

The splashing function f_d is not a constant. It is zero when the assist gas pressure is zero and progressively increases as the pressure increases. Since the gas pressure affects the melt velocity V_m, the splashing function is defined in terms of V_m as follows:

$$f_d=\frac{(1-X_d)V_m}{X_d v+V_m}, \tag{17}$$

TABLE II. Thermophysical properties of nitrogen.[a]

Thermophysical properties	Values of thermophysical properties
Pressure, P_0	1.013×10^{5}
Density, ρ_0 (300 K, 1 atm)	1.1233 kg m^{-3}
Kinematic viscosity, v_g (250 K, 1 atm)	11.48×10^{-6} m^2/s
Prandtl number, Pr (250 K, 1 atm)	0.727
Thermal conductivity, k_g (250 K, 1 atm)	22.2×10^{-3} W m^{-1} K^{-1}

[a]See Ref. 13.

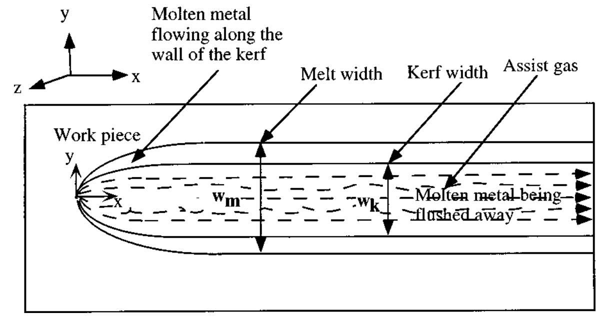

FIG. 2. Top view of the work piece showing how assist gas has squeezed metal along the wall of the kerf.

where X_d is a suitable constant. Utilizing Eqs. (10), (15), (17) and setting $w_k=w$ in Eq. (10), Eq. (16) can be written as

$$d_c=\left(\frac{-\left(\frac{dp}{dx}\right)w^2}{-\left(\frac{dp}{dx}\right)w^2+12X_d\mu v}\right)d_m. \tag{18}$$

III. MODEL FOR KERF WIDTH

The width of the slot, which is referred to as kerf width in laser cutting applications, produced due to melt removal by an assist gas is obtained by modifying the Rosenthal equation for temperature distribution.[20] The Rosenthal model is based on a point heat source, a semi-infinite workpiece, no heat losses due to convection and radiation, and no melting of the workpiece. To account for the reduction in temperature due to the melting of the workpiece and the removal of the superheated melt from the laser-material interaction zone, the Rosenthal equation is modified by incorporating a factor f_m, $0<f_m\leq 1$, as given below

$$T-T_0=\frac{PA}{2\pi k}\,e^{-vx/2\alpha}\,\frac{e^{-vr/2\alpha}}{r}, \tag{19}$$

where $r=\sqrt{x^2+y^2+z^2}$. The melt width is approximated by determining the width of the region at the substrate surface $(x=z=0)$ within which the temperature is above the melting temperature. To obtain a simple expression for the melt width w_m, r is set equal to $w_m/2$ in the denominator and is taken as $w/2$ in the exponent in Eq. (19), which reduces Eq. (19) to the following form:

$$w_m=f_m\,\frac{PA}{\pi k(T_m-T_0)}\,e^{-(vw/4\alpha)}. \tag{20}$$

Some of the molten material flows along the walls of the slot or kerf and most of it is splashed out by the assist gas (see Fig. 2). This produces a slot or kerf of width w_k which is related to the melt width w_m by the following mass balance equation:

$$\rho v w_m d_m \tau=\rho(V_m+v)(w_m-w_k)d_m\tau+f_w\rho v w_m d_m\tau. \tag{21}$$

The first term on the right hand side of this equation corresponds to the amount of material sticking along the kerf

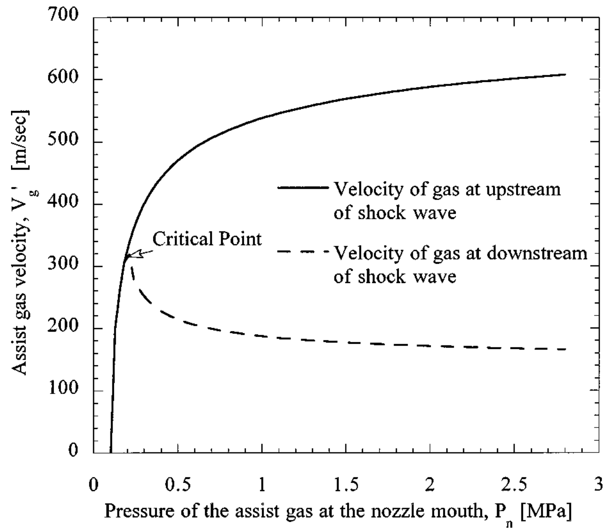

FIG. 3. Plot of Prandtl or Meyer relationship as a function of assist gas pressure at the nozzle mouth. The upper and lower curves indicate the velocity of gas at upstream and downstream side of the shock, respectively.

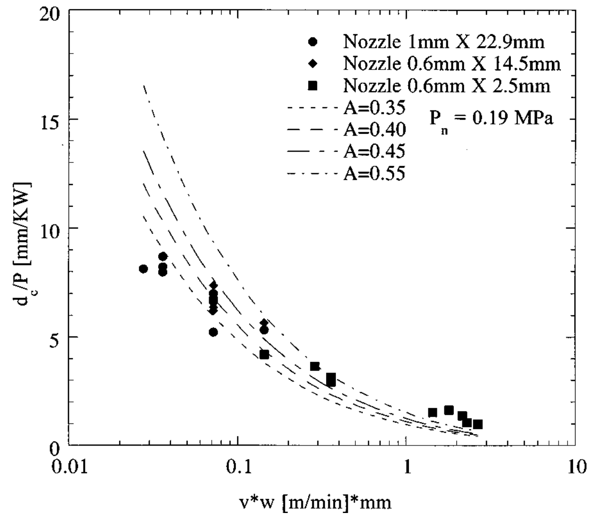

FIG. 4. Verification of the scaling law for cut depth with the experimental data.

walls while the second term represents the amount splashed out. Here f_w is a splashing function of similar nature as in the case of the cut depth. It is zero when the assist gas pressure is zero and increases progressively as the pressure increases. As in Sec. II, f_w is defined in terms of V_m in the following way:

$$f_w=\frac{(1-X_w)V_m}{X_w v+V_m}, \tag{22}$$

where X_w is a suitable constant. Utilizing Eqs. (10), (22) and setting $w_k=w$ in Eq. (14), the expression for the kerf width can be written as follows from Eq. (21):

$$w_k=\left(\frac{-\left(\frac{dp}{dx}\right)w^2}{-\left(\frac{dp}{dx}\right)w^2+12X_w\mu v}\right)w_m. \tag{23}$$

IV. RESULTS AND DISCUSSION

The melt and cut depths and the kerf width are calculated by using the above models and the data listed in Tables I and II. The results are compared with experimental data to verify the models. Details of the experimental set up and procedure have been presented in Ref. 1. The values of the parameters, F, X_d, f_m, and X_w are chosen to be $F=0.05$, $X_d=X_w=0.02$, and $f_m=0.27$ to obtain similar trends as experimental data. The physical meaning of choosing $X_d=X_w=0.02$ is that this choice leads to maximum cut depth over a wide range of cutting speed for sonic gas velocity at the inlet of the kerf of uniform width.

Figure 3 is a plot of the Prandtl or Meyer relation for the case in which the assist gas attains a critical speed at about 0.2 MPa gas pressure at the nozzle mouth and a shock wave is formed at an intermediate location between the nozzle and workpiece. The curve bifurcates at this critical speed. The upper curve represents the assist gas velocity at the upstream of the shock wave and the lower curve denotes the velocity downstream. The velocity of the downstream gas is always less than the critical speed of the gas. Figure 3 indicates that the velocity with which the assist gas enters the kerf decreases if a shock front is formed between the nozzle and workpiece. This reduces the effectiveness of the assist gas in removing the molten material.

Figure 4 shows the cut depth per unit power (d_c/P) as a function of the product of laser beam width and scanning velocity v. Four different absorptivity values in the range of 0.35 to 0.55 are used. The theoretical curves closely follow the experimental data and validates the theory. Figure 5 represents the variation in the cut depth with assist gas velocity at the nozzle exit. The curves show zero cut depth for zero gas velocity, rise sharply, and then attain constant values. This can be explained on the basis of the kerf geometry which is assumed to be nontapered through cut. Due to this the velocity of the assist gas remains equal to the critical value in the kerf even though the velocity of the gas may be supersonic outside the kerf. The curves indicate that the

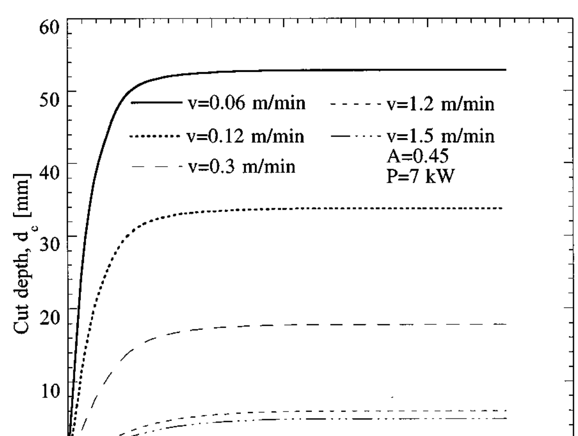

FIG. 5. Variation of cut depth with the assist gas velocity at the nozzle exit for different scanning velocities.

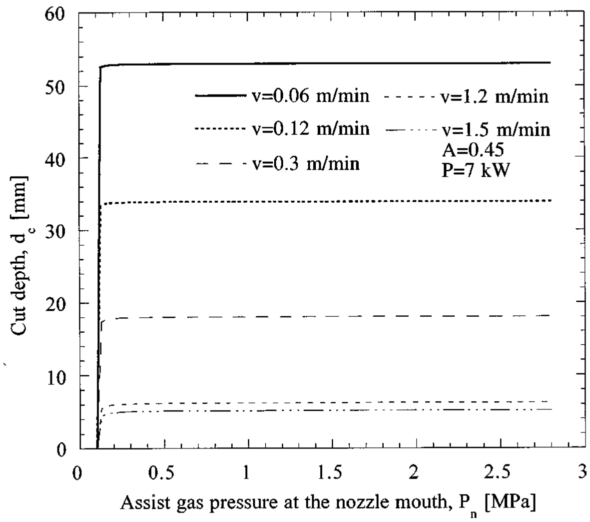

FIG. 6. Variation of cut depth with pressure of assist gas at the nozzle mouth at different scanning velocities.

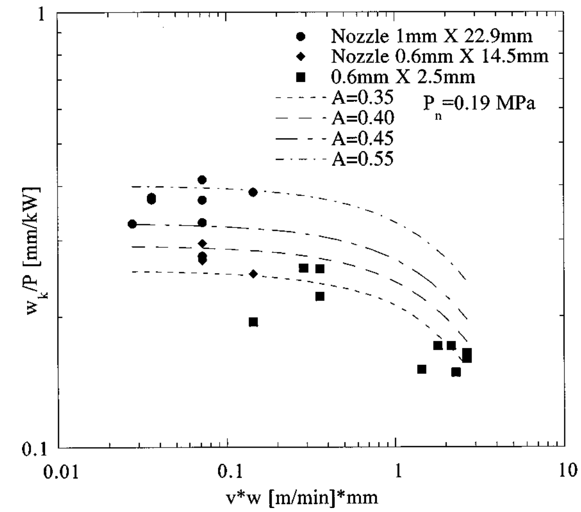

FIG. 8. Verification of scaling law for cut depth with experimental data.

maximum cut depth is achieved at gas velocities much lower than the critical speed. At higher scanning speeds the maximum cut depth is achieved at higher gas velocities though still less than the critical speed because the gas jet interacts with the workpiece for shorter duration. Figure 6 denotes the corresponding results in terms of the gas pressure at the nozzle mouth and essentially explains the same fact as in Fig. 5. Figure 7 shows the variation in the cut depth with the scanning velocity. The cut depth drops sharply for higher scanning speeds because the laser-material interaction time decreases and therefore, laser beam deposits less energy on the workpiece when the beam is scanned at the higher speeds.

The kerf width per unit power (w_k/P) is plotted against the product of the laser beam width w and the scanning velocity v in Fig. 8. Experimental data and model results show similar trends. Figures 9 and 10 examine the kerf width as a function of the assist gas velocity at the nozzle exit and pressure at the nozzle mouth, respectively. The kerf width rises sharply as the gas velocity or pressure increases, and then attains a constant value as the sonic velocity is approached due to the geometry of the kerf already mentioned above in the case of the cut depth (Fig. 5). Figure 11 shows that the kerf width decreases as the scanning velocity increases because of less energy deposition on the workpiece at higher scanning speeds.

Figure 12 examines the cutting speed as a function of the assist gas pressure at the nozzle mouth, and the model results are compared with experimental data taken from the Ref. 21. The results are shown for two cases involving 2 and 3 mm cut depths. The experimental data indicate that the cutting speed increases as the gas pressure is increased upto the critical pressure (0.2 MPa) and then drops on further increase of pressure. This trend is predicted by the present model on the basis of the assumption that a shock wave is formed at an intermediate location between the nozzle and workpiece for supersonic gas flow. The flow is then governed by the Prandtl or Meyer relation and the velocity of the gas at kerf inlet is always less than the critical velocity. In the pressure

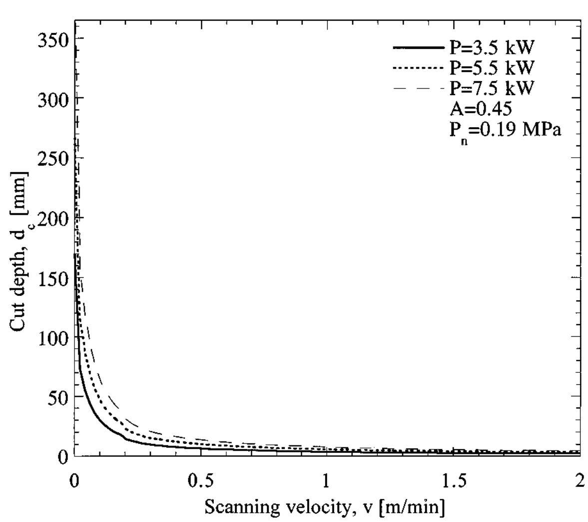

FIG. 7. Trends showing cut depth varying with the scanning velocity at different laser power.

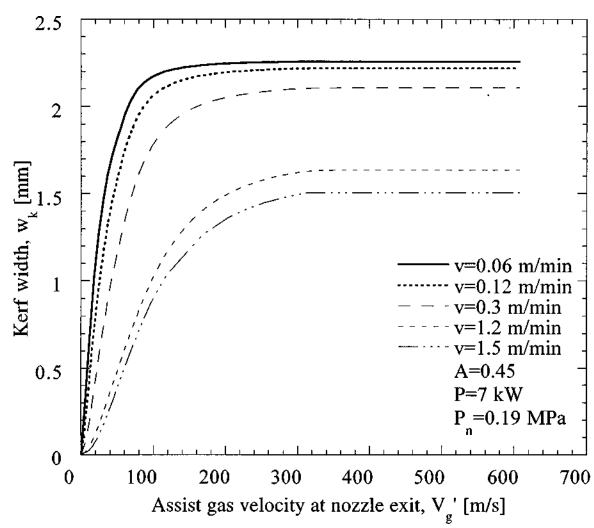

FIG. 9. Variation of kerf width with the assist gas velocity at nozzle exit for different scanning velocities.

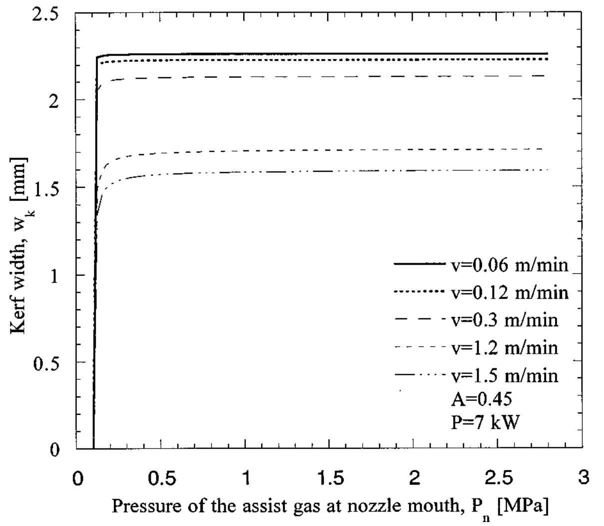

FIG. 10. Variation of kerf width with the assist gas pressure at the nozzle mouth for different scanning velocities.

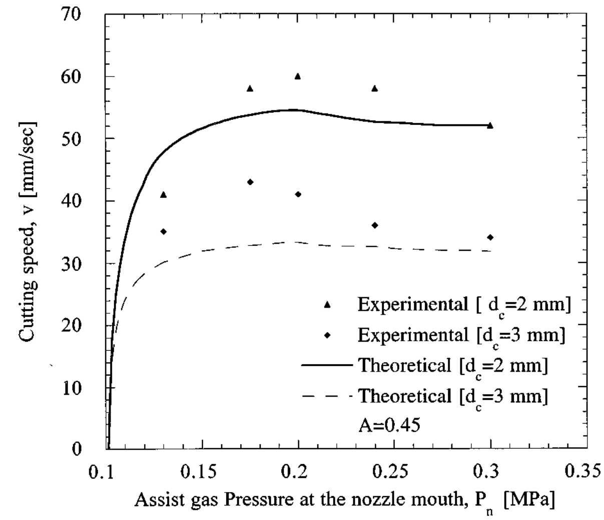

FIG. 12. Experimental data taken from Ref. 21 is compared with the theoretical results for 2 and 3 mm depths of cut, for a laser spot size of dimensions 0.25 mm×0.25 mm.

range $0.1<P_n<P^*=0.2$ MPa the velocity of the metal V_m is calculated on the basis of M_u^*, and V_m is determined by using M_d^* for $P_n \geqslant P^*$. It may be noted that the effective nozzle-to-plate distance becomes $H/2$ for supersonic gas flow because the shock wave is assumed to form halfway between the nozzle and workpiece. It is also assumed that the kerf is of nontapered geometry and that the size of the laser spot is 0.25 mm×0.25 mm. For this spot size X_d is chosen to be 0.0088.

V. CONCLUSIONS

Models for melt and cut depths and kerf width are presented for laser grooving and cutting applications. Experimental data for both cut depth and kerf width validate the model predictions. The cutting speed reaches a maximum value at a certain pressure of the assist gas. It decreases when the gas pressure is increased beyond the critical pressure for certain geometry of the kerf, and nozzle dimensions.

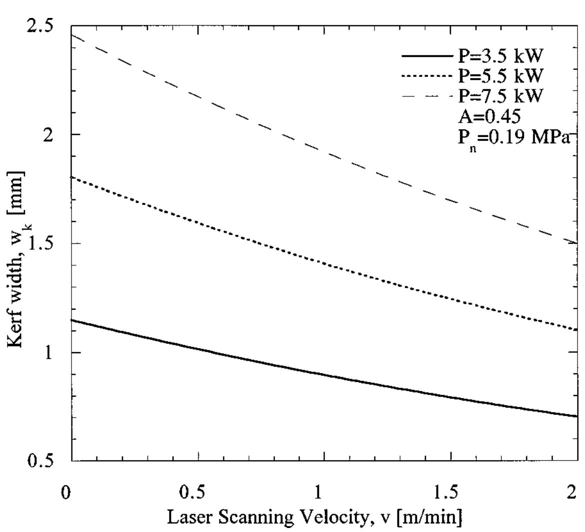

FIG. 11. Trends showing kerf width varying with the scanning velocity at different laser powers.

ACKNOWLEDGMENT

This work was done at the Center for Research and Education in Optics and Lasers (CREOL) in the University of Central Florida under AFSOR Contract No. F49620-93-C0063.

[1] A. Kar, J. E. Scott, and W. P. Latham, J. Laser Appl. **8**, 125 (1996).
[2] G. Chryssolourius and W. C. Choi, in *CO2 Lasers and Applications*, edited by J. D. Evansand and E. V. Locke (SPIE, Bellingham, WA, 1989), Vol. 1042, pp. 86–96.
[3] B. Biermann, S. Biermann, and H. W. Bergmann, J. Laser Appl. **3**, 13 (1996).
[4] P. A. Molian and M. Baldwin, J. Laser Appl. **4**, 9 (1992).
[5] D. Schuocker and W. Abel, in *SPIE Proceedings of the Industrial Applications of High Power Lasers* (SPIE, Bellingham, WA, 1984), Vol. 455, pp. 88–95.
[6] D. Schuocker, *The Industrial Laser Annual Handbook*, edited by D. Belforte and M. Levitt (PennWell Books, Tulsa, Oklahoma, 1987), pp. 65–79.
[7] M. F. Modest and H. Abakians, J. Heat Transfer **108**, 602 (1986).
[8] S. Y. Bang and M. F. Modest, J. Heat Transfer **113**, 663 (1991).
[9] S. Roy and M. F. Modest, Int. J. Heat Mass Transf. **36**, 3515 (1993).
[10] I. Belic and J. Stanic, Opt. Laser Technol. **19**, 309 (1987).
[11] I. Belic, Opt. Laser Technol. **21**, 277 (1989).
[12] A. Kar, J. A. Rothenflue, and W. P. Latham, J. Laser Appl. **9**, (1997).
[13] F. P. Incropera and D. P. DeWitt, in *Introduction to Heat Transfer*, 2nd ed. (Wiley, New York, 1990), pp. 402/403, A 20.
[14] A. G. Grigoryants, in *Basics of Laser Material Processing* (Chemical Rubber, Boca Raton, 1994), pp. 281–298.
[15] A. H. Shapiro, in *The Dynamics and Thermodynamics of Compressible Fluid Flow I* (Wiley, New York, 1953), pp. 73–158.
[16] I. G. Currie, in *Fundamental Mechanics of Fluids*, 2nd ed. (McGraw–Hill New York, 1993), pp. 354/355.
[17] W. F. Hughes and J. A. Brighton, in *Theory and Problems of Fluid Dynamics* (Schaum's Outline Series, New York, 1967), pp. 88/89, 116/117.
[18] E A. Brandes, in *Smithells Metal Reference Book* (Butterworth, Boston, 1983), pp. 14.7/14.8, 8.2, 14.1.
[19] L. M. Milne-Thomson, in *Theoretical Hydrodynamics*, 4th ed. (Macmillan, New York, 1966), pp. 149/150.
[20] D. Rosenthal, Welding J. (Miami) **20**, 220s (1941).
[21] W. M. Steen, in *Laser Material Processing* (Springer, London, 1991), pp. 89/90.